Jurnal Tribologi 48 (2026) 76-93

Jurnal Tribologi
MYTRIBOS Malaysian Tribology Society
Website : jurnaltribologi.mytribos.org e-issn: 2289-7232

Comparison of surface erosion between stainless steel 304 and carbon steel 1045 under waterjet peening process

Azmir Azhari [1*], Ahmad Shahir Jamaludin [1], Mebrahitom Gebremariam [2], Kushendarsyah Saptaji [3], Abdur-Rasheed Alao [4]

[1] Faculty of Manufacturing and Mechatronic Engineering Technology, Universiti Malaysia Pahang Al-Sultan Abdullah, 26600 Pekan, MALAYSIA.
[2] College of Engineering and Built Environment, Birmingham City University, B47XG Birmingham, UNITED KINGDOM.
[3] Faculty of Engineering and Technology, Sampoerna University, South Jakarta 12780, Jakarta, INDONESIA.
[4] Faculty of Engineering, Universiti Teknologi Brunei, Gadong BE1410, BRUNEI.
*Corresponding author: azmir@umpsa.edu.my

KEYWORDS

Waterjet impingement
Surface roughness
Hardness
Erosion mechanism
Stainless steel 304
Carbon steel 1045

ABSTRACT

This study presents a comparative evaluation of the erosion performance of stainless steel 304 (SS304) and carbon steel 1045 (CS1045) under waterjet peening process. The investigation focused on surface roughness and erosion characteristics under varying waterjet impingement parameters, including the number of jet passes, pressure, feedrate and stand-off distance. ANOVA results showed that the number of jet passes was the most influential parameter affecting surface roughness followed by pressure, feedrate and standoff-distance for both materials. In terms of surface roughness, CS1045 consistently exhibited greater value than SS304, primarily because of its lower hardness and reduced resistance to plastic deformation. Although CS1045 showed only slightly more severe material erosion overall, continuous surface degradation was particularly evident at higher pressures and increased jet passes. Hardness measurements further revealed that CS1045 exhibited a substantially greater increase in hardness compared to SS304 under identical waterjet conditions. Fractographic analysis revealed a predominantly ductile erosion mechanism in SS304, characterized by fibrous and dimpled fracture surfaces. Conversely, CS1045 displayed a mixed brittle–ductile erosion mode, with cleavage features and river patterns indicative of brittle fracture. These observations highlight the complex nature of material response to waterjet impact, where factors such as microstructure, hardness, and energy absorption mechanisms significantly influence erosion behaviour. The findings offer valuable insights for selecting suitable materials in applications involving high-pressure fluid impact and surface treatment processes.

Received 28 July 2025; received in revised form 12 December 2025; accepted 26 December 2025.
To cite this article: Azhari et al. (2026). Comparison of surface erosion between stainless steel 304 and carbon steel 1045 under waterjet peening process. Jurnal Tribologi 48, pp.76-93.

1.0 INTRODUCTION

In recent decades, surface engineering has appeared to be extremely important in the progress and life-cycle optimization of structural materials. Among the many surface modification methods, waterjet surface treatment or waterjet peening (WJP) has attracted considerable interest because it is environmentally sustainable and does not introduce thermal effects. Unlike traditional shot peening or laser peening, waterjet peening utilizes high-pressure water jets to induce compressive residual stresses, improve surface hardness, and enhance fatigue performance without introducing thermal distortion or contamination (Aida Husna Mohd Mahayuddin et al., 2020; Qutaba et al., 2022). It is particularly advantageous for treating complex geometries and temperature-sensitive components.

The effect of waterjet peening on different metallic materials has been widely studied, with research focusing on both the beneficial modifications and potential erosion damage caused by prolonged or aggressive jet exposure. Waterjet peening increases near-surface hardness in metallic alloys and produces microstructural deformation (Azhari et al., 2012; Barletta, 2011). In the context of ferrous alloys, materials such as austenitic stainless steel and medium-carbon steels are commonly employed in structural and industrial applications due to their mechanical strength, corrosion resistance, and cost-effectiveness (Bringas, 2004). Austenitic stainless steels are widely used due to their excellent formability, even at room temperature (Bigdeli Karimi et al., 2008). Among these, SS304 is the most common grade and is extensively applied in chemical processing equipment, heat exchangers for the food, dairy, and beverage industries, as well as in medical devices (Rossi et al., 2024). In contrast, CS1045 is a medium-carbon steel that responds well to heat treatment processes (Lesyk et al., 2019). Heat-treated CS1045 exhibits improved strength, making it suitable for demanding applications such as railway wheels and rails, gears, crankshafts, and other machine components or structural parts that require a balance of high strength, wear resistance, and toughness (Naeem et al., 2022a). However, these materials respond differently to surface impingement processes owing to their distinct microstructural and mechanical characteristics. The impact mechanism of a waterjet is largely influenced by how the jet stream interacts with the material surface. The physical attributes of the waterjet such as velocity, coherence, and focus play a crucial role in determining the surface response of the material being treated. As such, it is essential to understand the behaviour and structure of the waterjet flow from the point it leaves the nozzle to the moment it strikes the workpiece.

It is well established that water under high pressure can cause significant surface erosion on solid materials. This damage results from the collision of high-velocity water masses with the material surface, generating intense, short-duration pressure pulses. According to a comprehensive review by Field (1999), liquid impact on a solid target can be divided into two distinct stages. In the initial stage, the liquid behaves compressibly, producing a transient yet extremely high pressure known as the "water-hammer" or impact pressure (Shen et al., 2023). When the droplet contacts the surface, a shock front forms, leading to localized compressive stress—this is the primary cause of surface damage. The second stage follows the release of this pressure, during which a rapid pressure drop occurs around the contact edge. Collectively, both stages contribute significantly to the material erosion process.

Austenitic stainless steel 304 (SS304) is characterized by a face-centered cubic (FCC) crystal structure, offering excellent ductility, corrosion resistance, and work-hardening capabilities. Under waterjet peening, SS304 exhibits surface strengthening primarily through strain-induced plastic deformation and phase transformation (e.g., martensitic transformation). Previous studies have shown that waterjet peening can significantly enhance the surface hardness and fatigue performance of SS304 with minimal material loss (Qutaba et al., 2022; Yun et al., 2020). On the other hand, carbon steel 1045 (CS1045), a medium-carbon steel with a body-centered cubic (BCC) structure, displays higher initial hardness and strength but is less ductile and more prone to brittle erosion mechanisms (K. Wang et al., 2024). Earlier research indicated that prolonged exposure of CS1045 to waterjet impingement leads to substantial surface erosion, including pitting, micro-cracking, and material fragmentation (Rasse et al., 2021). While this material can benefit from peening-induced surface compressive stresses, its limited plasticity and erosion resistance under high-velocity jets pose challenges for long-term surface integrity.

A comparison with previous studies shows that earlier work typically focused on either surface hardening or erosion behaviour in isolation and often investigated only a single material or a narrow range of parameters. For example, Azhari et al. (2012) demonstrated the capability of waterjet peening to improve the surface hardness of stainless steel but did not evaluate erosion responses or compare performance across different materials under identical jet conditions. The subsequent study by Azhari et al. (2014) examined erosion behaviour in CS1045 however no cross-material comparison was performed, limiting direct interpretation of material-dependent response. Similarly, broader erosion models proposed by Oka et al. (2007) and cavitation-induced surface modification reported by Krella (2005) were conducted under different hydrodynamic regimes and did not evaluate matched conditions across materials. In contrast, the present study provides the first direct, systematic comparison of SS304 and CS1045 under identical waterjet operating conditions, allowing a clear evaluation of the intrinsic material sensitivity to jet-induced erosion. The expanded parameter matrix namely pressure, standoff distance, feed rate, and number of passes offer a substantially broader parametric domain than most previous works, enabling multivariate assessment of process interactions. Furthermore, the inclusion of statistical analyses (ANOVA) and quantitative hardness profiling establishes a level of analytical rigor does not present simultaneously in earlier studies. Importantly, the results reveal material-specific erosion mechanisms and process severity thresholds that have not been reported previously. This integrated approach not only clarifies the mechanisms governing material-specific erosion but also highlights parameter combinations that offer practical advantages in terms of process efficiency and economic applicability.

This gap in knowledge limits the ability of engineers and designers to make informed decisions regarding material selection for components exposed to fluid erosion, such as turbine blades, pump impellers, and marine structures. The objective of this study is to bridge this gap by directly comparing the surface erosion behavior of SS304 and CS1045 under identical waterjet surface impingement parameters. This comparative study will provide valuable insights into the erosion tolerance of these widely used materials, thus supporting more effective design strategies for waterjet-based surface treatments and applications exposed to high-velocity fluid environments.

2.0 METHODOLOGY

This study presents a comparative analysis on two commonly used ferrous alloys, stainless steel 304 (SS304) and carbon steel 1045 (CS1045). Both materials were subjected to waterjet surface impingement under identical processing conditions. All procedures, parameters, and evaluation methods were kept consistent to ensure reliable comparison of erosion behavior.

SS304 is a non-magnetic, corrosion-resistant steel alloy with a face-centered cubic (FCC) crystal structure. The material used in this study had the following nominal chemical composition (wt.%): 18.0–20.0% Cr, 8.0–10.5% Ni, ≤0.08% C, with the remainder being iron (Bansod et al., 2018). Its austenitic structure offers excellent ductility and strain-hardening capacity, making it suitable for mechanical and thermal processing. CS1045 is a medium-carbon steel with a body-centered cubic (BCC) structure, known for its moderate strength and hardness. The typical chemical composition includes 0.43–0.50% C, 0.60–0.90% Mn, and trace amounts of P and S (Naeem et al., 2022b). Unlike SS304, CS1045 has limited corrosion resistance and lower ductility, which can influence its erosion resistance under dynamic surface treatment (Azhari et al., 2014). The typical mechanical properties of as-received specimens for both SS304 and CS1045 are shown in Table 1.

Table 1: Mechanical properties of SS304 and CS1045 (Bringas, 2004).

Material	Yield strength (MPa)	Tensile strength (MPa)	Elongation (%)
SS304	230	540-750	45
CS1045	230-305	530-580	15-16

Surfaces of the received specimens were prepared with the dimension of 150 mm x 30 mm and surface roughness, R_a of 0.15 µm and 0.07 µm respectively for SS304 and CS1045. The cross-sectioned microstructures show the equiaxed grain structures for SS304 and ferrite and pearlite constituents for CS1045 as revealed in Figure 1. For SS304, the as-received specimens had already been smoothed and film-coated during production through the rolling process. In contrast, the as-received CS1045 specimens exhibited a relatively rough surface from rolling; therefore, additional surface preparation was required. These specimens were polished to a mirror-like finish using a lapping machine, achieving a very low average surface roughness, R_a of 0.07 µm. The surface hardness of both materials was measured using a computer-controlled Buehler OmniMet MHT tester, with Vickers hardness determined under a 10 gf load and a 15 s dwell time. At least four indentations were averaged for each material, giving hardness values of 230 $HV_{0.01}$ for SS304 and 145 $HV_{0.01}$ for CS1045. The lower hardness observed for CS1045 compared to literature values can be attributed to the lapping process, which is known to reduce apparent hardness by removing work-hardened surface layers and modifying the near-surface microstructure (Rudawska, 2014).

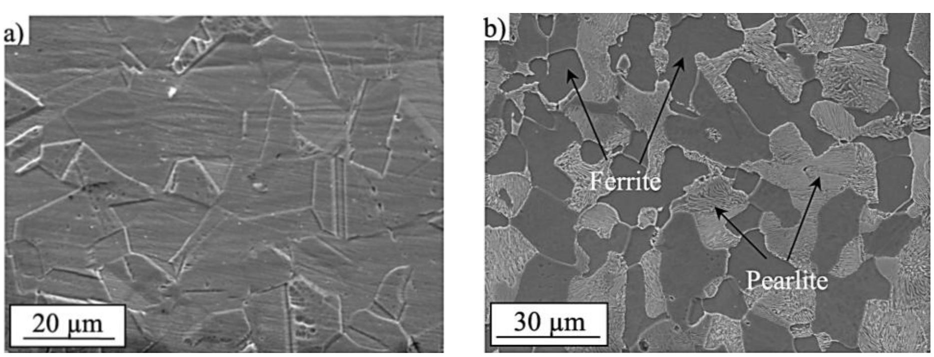

Figure 1: Cross-sectioned microstructures for, a) SS304 and b) CS1045.

UHDE high pressure waterjet machine was used as the equipment for machining all the samples. The machine can generate up to 600 MPa of the water pressure with a maximum flow rate of about 2 l/min. The nozzle head was set perpendicular to the specimen surface at 90°. A 0.3 mm sapphire nozzle was used, resulting in about 0.8 mm of a treated width. The process was carried out without any abrasive additives, ensuring that the treated surfaces remained free from embedded abrasive particles.

In this study, four key machining parameters were selected for evaluation. These parameters were easily adjustable and could be precisely controlled at the desired levels. Table 2 shows the machining parameters and their ranges. The selected ranges (100–300 MPa, 2–6 passes, 1000–3000 mm/min, 30–180 mm standoff) are consistent with previous works by (Azhari et al., 2012, 2014), where cavitation intensity and surface strengthening occurred within similar operating windows. These ranges are also representative of industrial waterjet peening conditions, where energy delivery is controlled by pressure, jet coherence (via standoff distance), and exposure time (via passes and feed rate).

Table 2: Machining parameters and their ranges.

No.	Machining parameters	Ranges
1.	Number of jet passes, *n*	2 – 6
2.	Pressure, *p* (MPa)	100 – 300
3.	Feedrate, *v* (mm/min)	1000 – 3000
4.	Stand-off distance, *h* (mm)	30 – 180

Quantifying the severity of the jet conditions and enable comparison of different pressure levels, the energy delivered to the surface was expressed in terms of energy density. In this study, the energy density represents the mechanical power of the jet distributed over the nozzle exit area, providing a measure of the effective impact intensity. It was calculated using Equation 1 (Hashish, 2024).

$$E = \sqrt{\frac{2}{\rho_o}} C_d P^{1.5} \quad (1)$$

where ρ_o is the water density, C_d is the orifice coefficient of discharge, P is the operating pressure. In this study, the resulting energy densities increased substantially with pressure, ranging from approximately 4 W/cm^2 at 100 MPa, to 16 W/cm^2 at 200 MPa, and 36 W/cm^2 at 300 MPa, demonstrating the strong nonlinear amplification of jet energy with increasing pressure. These calculated values provide a clearer engineering perspective on the severity of the tested conditions and help contextualize the observed differences in surface erosion behaviour between the materials.

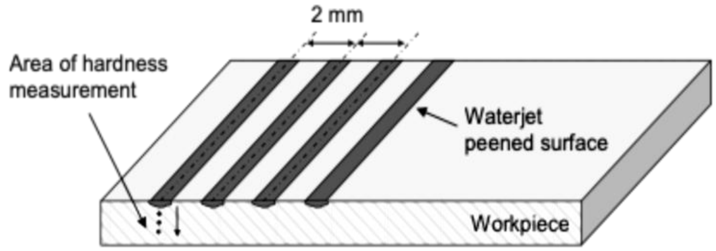

Figure 2: Illustration of the treated specimen.

The workpiece was positioned on the worktable of the machine and securely clamped to maintain a fixed horizontal orientation throughout the experiment. For each trial, every parameter was adjusted according to the predefined experimental design. Once all parameters were configured, the treatment was carried out following a programmed CNC routine. The nozzle traversed across the width of the specimen, as illustrated in Figure 2, and moved back and forth repeatedly based on the specified number of jet passes. A 2 mm spacing was maintained between each treatment track to prevent overlap or interference between adjacent waterjet paths.

All treated surfaces were thoroughly analysed. Part of the treated surface was allocated for surface roughness evaluation, while a separate area was reserved for microstructural analysis to prevent any interference caused by the contact-based roughness measurement. The surface roughness was assessed using a computer-controlled device (Hommel T8000) equipped with a ball-shaped ruby stylus featuring a 5 μm tip diameter and a 90° tip angle. The transverse surface roughness profiles were measured at the center of each treated track. All measurements were performed using a cut-off length of 0.8 mm, and the average roughness (*Ra*) was evaluated following the ISO 4287 standard. To improve reliability and minimize measurement variability, each sample was assessed at least four times, and the results were averaged. Microstructural examination was carried out using a scanning electron microscope (Philips XL 40) operated at an accelerating voltage of 20 kV. Secondary Electron Imaging (SEI) was primarily utilized for capturing microstructural details, with magnification levels adjusted as needed to observe both macro- and micro-scale features. In this study, ANOVA analysis was conducted using the Minitab® Statistical Software for all experimental design parameters, with models and outputs considered as response variables. The percentage effect ratios were also examined.

The treated specimens underwent preparation for standard hardness measurement and microstructural analysis. A computer-controlled Buehler OmniMet MHT hardness tester was used to conduct subsurface Vickers hardness measurements on the polished cross-sections, with the procedure depicted in Figure 2. A consistent load of 10 gf was applied for 15 seconds during each indentation. To ensure accuracy, at least four hardness data points were averaged at each specific depth. Measurements were systematically taken at 10 increasing depths, starting from roughly 25 μm below the eroded surface and continuing until a far distance of 1000 μm (specifically at 25, 50, 75, 100, 150, 200, 300, 500, 750, and 1000 μm).

3.0 RESULTS AND DISCUSSION

Table 3 shows the ANOVA results for the surface roughness *Ra*. The analysis was carried out for a 95 % confidence level. The ANOVA results show that number of jet passes is the most dominant factor influencing the response variables which contributes 51% of the overall effect ($F = 29.66$, $p < 0.001$). A higher F-statistic indicates that a greater proportion of the total variation in performance can be explained by changes in the process parameter (Kara et al., 2025). Also, if a model and its constituent terms each have a p-value of 0.05 or less, this indicates that those terms have a statistically significant influence on the response variable (Öztürk and Kara, 2025). Therefore, it can be said that variations in the number of passes cause substantial changes in surface roughness. Among the main effects, pressure (9.61% effect, $p = 0.056$) and feedrate (7.79% effect, $p = 0.099$) exhibit moderate contributions, although their p-values indicate borderline or marginal significance at the 5–10% level. Standoff distance also contributes noticeably at 14.51%, but the factor is statistically non-significant ($p = 0.122$), suggesting that its influence is present but inconsistent across the tested ranges. Material type shows the smallest effect among the main factors (3.54%) and is statistically non-significant ($p = 0.15$), indicating that the material does not substantially affect the observed response under the tested conditions. For interaction effects, the pressure × number of jet passes interaction is statistically significant (F = 10.79, p = 0.002) and contributes 4.61% to the total effect, revealing that the influence of pressure depends on how many passes are applied. Meanwhile, the feedrate × number of jet passes interactions shows a small contribution (1.34%) and is not statistically significant (p = 0.082). The error term accounts for a relatively small portion of total variation (48.21 out of 634.9 total SS), indicating good model fit. Overall, the results confirm that number of passes is the most influential factor, with pressure, standoff distance, and feedrate contributing secondary but noteworthy effects, while material type plays a minimal role in this study.

Table 1: ANOVA results for surface roughness (Ra).

Source	DF	Adj SS	Adj MS	*F*-Value	*P*-Value	% Effect
Material	1	22.47	22.47	2.13	0.15	3.54
Number of jet passes	2	323.8	161.894	29.66	0	51.00
Pressure	2	61.01	30.51	3.03	0.056	9.61
Feedrate	2	49.46	24.73	2.41	0.099	7.79
Standoff Distance	5	92.12	18.42	1.83	0.122	14.51
Feedrate*No. of passes	1	8.528	8.5284	3.14	0.082	1.34
Pressure*No. of passes	1	29.3	29.2995	10.79	0.002	4.61
Error	45	48.212	10.05			
Total	59	634.9				

This study compares the surface roughness and erosion behaviour of SS304 and CS1045. In surface roughness evaluation, it is common practice to report the mean value together with the standard deviation as mean ± standard deviation. In the present study, for SS304, the overall roughness across all runs was 3.93 ± 3.42 µm, with run-level means ranging from 0.73–13.22 µm and standard deviations of 0.11–1.61 µm. For CS1045, the overall roughness was 2.83 ± 2.94 µm, with run-level means of 0.26–8.93 µm and standard deviations of 0.06–1.09 µm. Run-level standard deviations were generally smaller for CS1045 (i.e. 0.06–1.09 µm) compared to SS304 (i.e. 0.11–1.61 µm), indicating that CS1045 exhibited more consistent machining performance (Palová et al., 2023).

Overall, CS1045 exhibited higher surface roughness values than SS304, as illustrated in Figures 3, Figure 4, and Figure 5. This outcome is expected due to the lower hardness of CS1045, which reduces its resistance to erosion and results in greater surface texture changes. Interestingly, the increase in surface roughness for CS1045 was relatively moderate when compared to SS304 under the same processing conditions, despite its hardness being just over half that of SS304. Furthermore, erosion in CS1045 was only marginally more pronounced, with a smoother and more continuous eroded surface especially at elevated pressures and with a higher number of jet passes, as shown in Figure 6, compared to the less continuous erosion seen in SS304 (Figure 7). One possible explanation is the initially smoother surface of CS1045 (0.07 µm) compared to SS304 (0.15 µm), which may have contributed to the lower increase in roughness following waterjet treatment. It is well established that smoother initial surfaces tend to enhance erosion resistance (Preece and Draper, 1981).

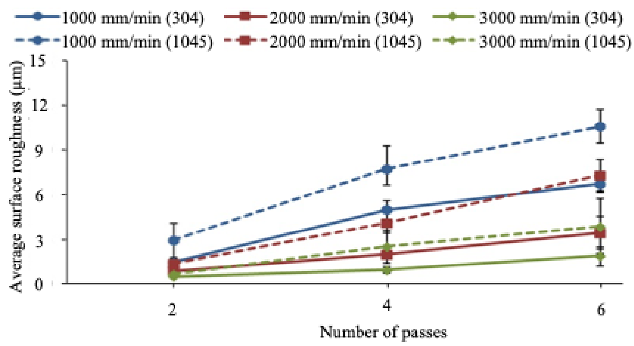

Figure 3: Influence of jet pass count on surface roughness at various feedrates, with a fixed pressure of 200 MPa and 30 mm standoff distance (SS304 shown as solid lines, CS1045 as dashed lines).

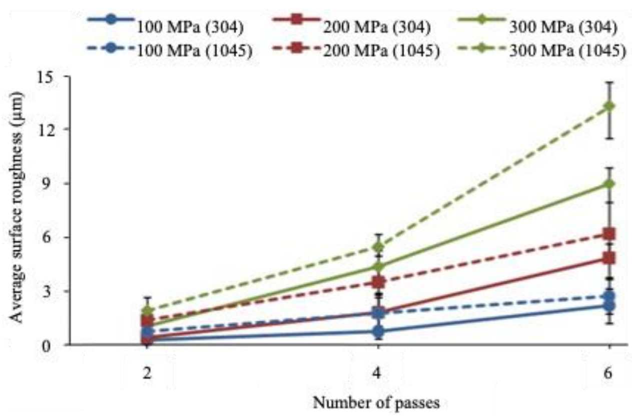

Figure 4: Influence of jet pass count on surface roughness at various pressures, with a fixed feedrate of 2000 mm/min and 30 mm standoff distance (SS304 shown as solid lines, CS1045 as dashed lines).

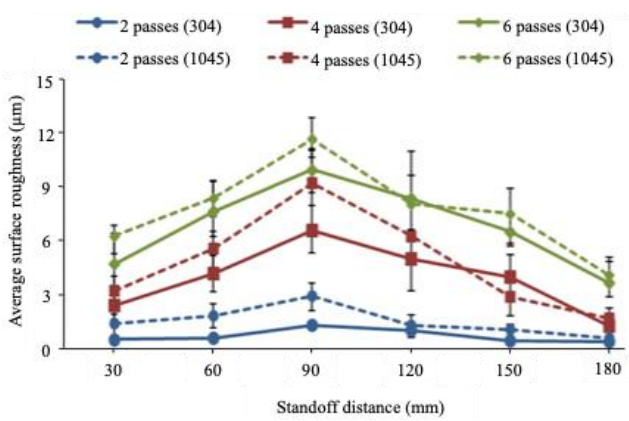

Figure 5: Influence of jet pass count on surface roughness at various number of jet passes, with a fixed pressure of 200 MPa and 2000 mm/min feedrate (SS304 shown as solid lines, CS1045 as dashed lines).

Figure 5 illustrates the influence of standoff distance on surface roughness at varying numbers of jet passes during the waterjet peening process. Initially, surface roughness increases as the standoff distance grows, reaching a peak at approximately 90 mm. Beyond this point, roughness begins to decline and gradually returns toward the untreated surface condition. At very short standoff distances, minimal material removal occurs likely due to the formation of a continuous water column rather than discrete water droplets (Oka et al., 2007). This continuous stream exerts compressive force on the surface without generating the cyclic impacts necessary for erosion. As a result, the frequency and intensity of impacts are insufficient to cause notable surface damage.

Additionally, at shorter distances, reflected water may interfere with incoming jets, further reducing erosion effect (Zhuang et al., 2022). At greater standoff distances, jet divergence minimizes this reflection, allowing for more effective droplet impingement. The range between 60 mm and 120 mm appears to represent a transition zone, where the jet changes from a continuous flow to discrete droplets (Zhuang et al., 2022). Previous studies have reported peak erosion effects within this range. Han et al. (2007) noted maximum cavitation pressure between 70 and 95 mm. However, further increases in standoff distance reduce erosion due to lower droplet velocity and energy dissipation. At this stage, the jet loses sufficient impact force to significantly alter the surface, resulting in decreased roughness. As noted by Noor Fatihah Mohamad et al. (2024), maintaining an optimal, relatively short standoff distance is crucial for achieving uniform surface features and improved finish quality.

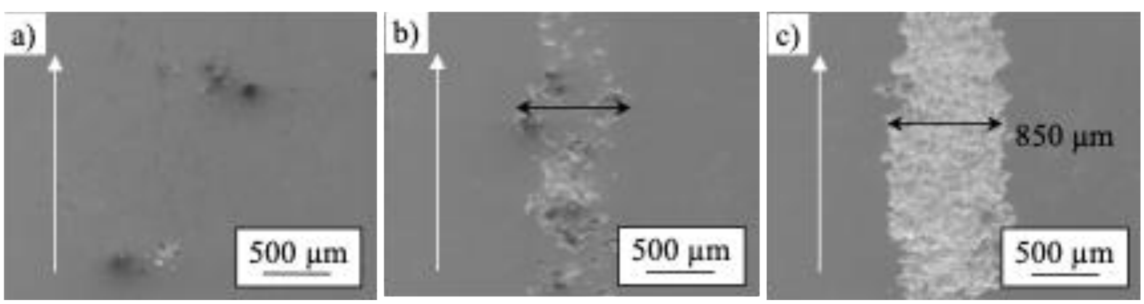

Figure 6: Erosion tracks of CS1045 for various number of jet passes, a) 2 passes, b) 4 passes and c) 6 passes, conducted under a pressure of 300 MPa, 2000 mm/min feedrate and 30 mm standoff distance.

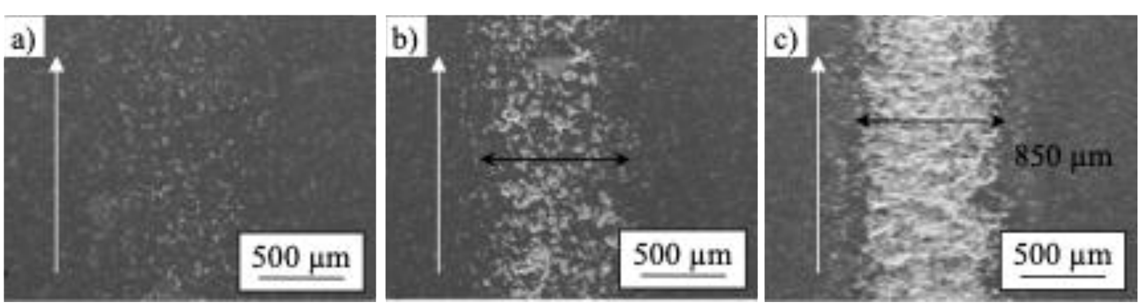

Figure 7: Erosion tracks of SS304 for various number of jet passes, a) 2 passes, b) 4 passes and c) 6 passes, conducted under a pressure of 300 MPa, 2000 mm/min feedrate and 30 mm standoff distance.

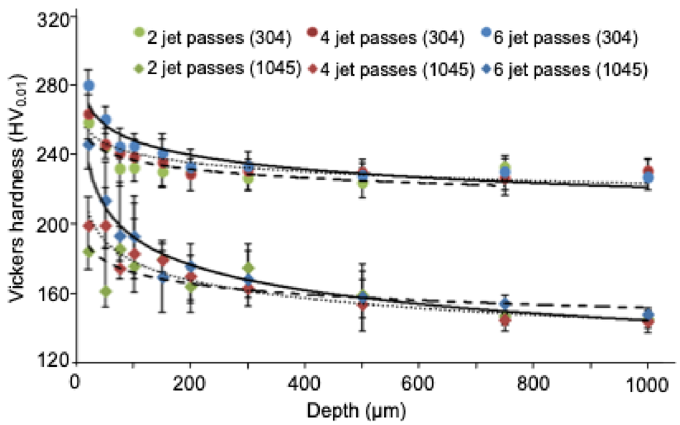

Figure 1: The impact of the number of jet passes on Vickers hardness at different depths below the surface at *p* = 200 MPa, *v* = 2000 mm/min, and *h* = 30 mm.

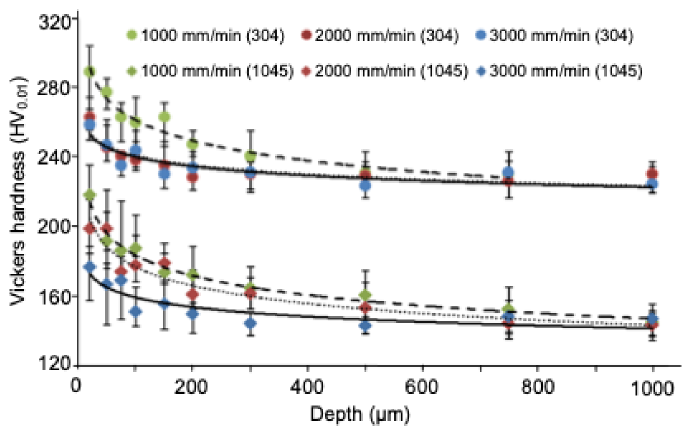

Figure 2: The impact of feedrate on Vickers hardness at different depths below the surface at *p* = 200 MPa, *n* = 4, and *h* = 30 mm.

Hardness measurements were taken from the surface down to a depth of 1000 μm to study how repeated jet impacts (passes) affect two different metals: SS304 and CS1045 (see Figure 8). For SS304, significant hardening was mostly confined to the top 100 μm, though more passes might push this depth slightly to 150 μm. More passes led to greater hardening. The average maximum hardness increased from 258 $HV_{0.01}$ (2 passes) to 280 HV0.01 (6 passes). This represents a 12% to 22% increase over the original base material hardness of about 230 $HV_{0.01}$. CS1045 showed hardening effects extending much deeper, up to about 300 μm, before returning to its original hardness of roughly 145 $HV_{0.01}$. Like SS304, more passes resulted in higher maximum hardness readings, increasing from 184 $HV_{0.01}$ (2 passes) to 246 $HV_{0.01}$ (6 passes). This translates to a more dramatic percentage increase: 27% to 70% above the base material's hardness. In both materials, more jet passes clearly produce both a harder surface and a deeper hardened layer. This is caused by work hardening from repeated water droplet impacts. The initial increase in hardness likely improves the material's initial resistance to erosion. Prolonged exposure can cause this brittle hardened layer to chip away, potentially increasing the overall erosion rate over time (Duraiselvam et al., 2007). Although the layer is repeatedly impacted, it appears that new hardening occurs with subsequent passes rather than the entire layer being removed immediately.

Figure 9 illustrates the inverse relationship between the feedrate and the resulting subsurface hardness profile in which slower feedrates lead to greater hardening effects. This trend holds true for both SS304 and CS1045, where the highest hardness increases were achieved using the slowest feedrate of 1000 mm/min (a 27% increase for SS304 and a 50% increase for CS1045). This slower rate also resulted in deeper hardening layers (300 µm for SS304 and 400 µm for CS1045). Faster rates above a certain threshold (e.g., 2000 mm/min and 3000 mm/min for stainless steel) yielded diminishing and overlapping results, confirming that reduced traverse speed allows for more water impacts, thus introducing beneficial compressive stresses and increasing overall hardness and hardening depth (Azhari et al., 2016).

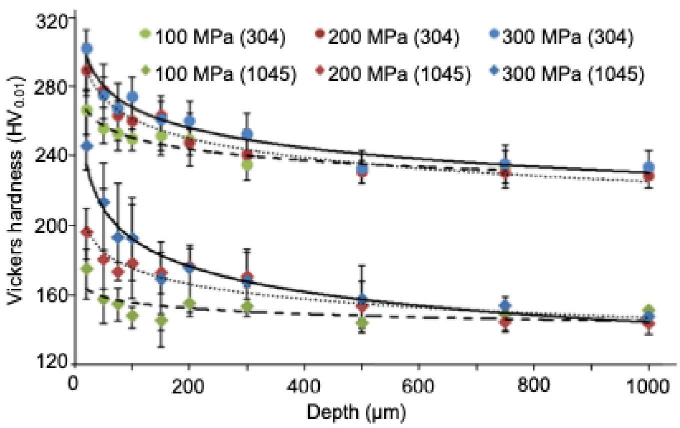

Figure 3: The impact of pressure on Vickers hardness at different depths below the surface at v = 0200 mm/min, n = 4, and h = 30 mm.

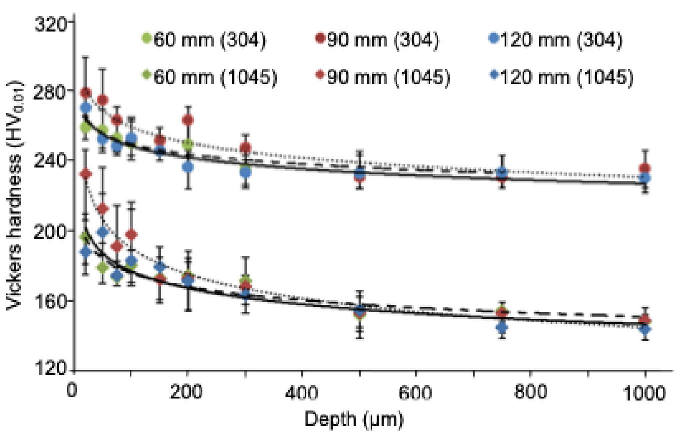

Figure 4: The impact of standoff distance on Vickers hardness at different depths below the surface at p = 200 MPa, v = 2000 mm/min, and n = 4.

Figure 10 illustrates that higher treatment pressure increases both the surface hardness and the depth of the hardened layer for both SS304 and CS1045. In both materials, hardness is highest at the surface and decreases with depth. For SS304, increasing the pressure from 100 MPa to 300 MPa increased the maximum hardness by 16% to 31%, with hardening effects reaching depths up to 250 μm. For CS1045, the impact was more significant, resulting in maximum hardness increases of 21% to 70%, and a hardening depth of 300 μm. This effect occurs because higher pressure translates to greater kinetic energy in the water impacts, inducing more compressive stress and plastic deformation in the material (Azhari et al., 2012). The lowest pressure of 100 MPa had minimal effect on CS1045, suggesting that the water droplets lacked sufficient energy to permanently deform the surface at that pressure level.

Figure 4 demonstrates the effect of standoff distance (distance from nozzle to material) on subsurface hardness. In both SS304 and CS1045, the hardness consistently decreased from the surface downwards. The optimal standoff distance for maximizing surface hardening in both materials was found to be 90 mm, as this distance likely generates the highest impact pressure. For SS304, the 90 mm distance increased maximum hardness by 21% (compared to 13% at 60 mm and 18% at 120 mm), with hardening effects limited to depths less than 200 μm. For CS1045, the 90 mm distance resulted in a 60% increase in hardness (compared to 34% at 60 mm and 37% at 120 mm), with hardening reaching depths up to 300 μm.

Comparing the two materials, CS1045 consistently showed a much higher percentage increase in hardness (up to 70%) than SS304 (maximum 31%) under the same treatment parameters. This difference is primarily due to CS1045 being significantly softer initially (145 $HV_{0.01}$ vs. 230 $HV_{0.01}$ for SS304). The softer material experiences greater plastic deformation and cold work during the waterjet impact, allowing for a larger relative increase in hardness (Mahagaonkar et al., 2008). Furthermore, CS1045 measurements showed a wider variation in hardness data compared to the stable results from SS304. This stability in stainless steel is attributed to the formation of a hard, stable martensite phase during the work hardening process (Nikitin & Besel, 2008). The high variability in CS1045 likely results from its mixed microstructure (soft ferrite and harder pearlite phases), where the small indenter load hits different phases, causing inconsistent readings. While the trend in this study aligns with literature (carbon steel hardens more than stainless steel under peening processes), the overall magnitude of hardness increase achieved in the current waterjet process is lower than that reported for traditional shot peening or laser shock peening methods (Avilés et al., 2011; Hacini et al., 2008; Zhan et al., 2012).

Material properties such as strength, hardness, ductility, and fatigue resistance are well-known to influence surface erosion behavior. According to Krella (2023), an increase in strength and hardness generally enhances resistance to cavitation erosion. However, the correlation between hardness and the incubation period (i.e. the time before significant material loss begins) is not always direct. This is consistent with the findings of the present study, where despite SS304 exhibiting greater hardness (230 $HV_{0.01}$) compared to CS1045 (145 $HV_{0.01}$), both materials showed similar incubation periods (2–4 jet passes), as observed in Figures 3 and Figure 4. Erosion under waterjet impact is a complex phenomenon affected by numerous variables. A lower hardness does not necessarily equate to reduced erosion resistance. As noted by Cao et al. (2022), no straightforward relationship exists between cavitation-induced material loss and mechanical properties such as strength or toughness. While Krella (2023) found a general trend of decreased erosion with increased hardness, this does not apply universally particularly in dual-phase alloys, where microstructural constituents such as primary ferrite play a more critical role than hardness alone. Mann & Arya (2002) also emphasized the importance of surface hardness, particularly during the early (incubation) stage of erosion, in coated materials.

Wang et al. (2024) suggested that erosion rates are strongly influenced by cyclic deformation behavior, indicating a fatigue-related mechanism. Their research demonstrated that erosion depth is inversely related to the fatigue strength coefficient. SS304, having a higher fatigue strength coefficient than CS1045, correspondingly exhibits superior erosion resistance (Richman & Mcnaughton, 1990). Further, Feller and Kharrazi (1984) noted that binding energy and crystal structure are key determinants of erosion behavior. Alloys with a single phase and low stacking fault energy, like SS304, tend to deform via planar slip, which localizes damage along grain boundaries and limits erosion (Hu et al., 2022).

In contrast, multi-phase alloys like CS1045 are more prone to erosion due to differential deformation between phases. Cracks often initiate at phase interfaces, leading to preferential removal of second-phase particles and lateral growth of flat-bottomed pits (Preece & Draper, 1981). These processes concentrate stress near the surface, increasing crack formation. This explains the higher erosion observed in CS1045, which contains ferrite and pearlite, compared to the single-phase austenitic structure of SS304. Additionally, the Body-Centered Cubic (BCC) structure of ferritic steels is more sensitive to strain rate. The high strain rates from waterjet peening promote rapid brittle fracture along both intergranular and transgranular paths (Shibata et al., 2022). Another key factor in SS304's erosion resistance is its ability to undergo phase transformation during waterjet impact. This transformation, from austenite to martensite, absorbs energy and enhances work hardening (A. K. Krella, 2023). The energy from localized droplet impacts facilitates dislocation movement and structural transformation, further increasing erosion resistance. Overall, such phase and dislocation changes alter the mechanical response and contribute to improved durability under erosive loading.

SEM analysis at higher magnifications further confirmed erosion mechanisms. Although both materials are ductile, distinct damage patterns emerged. In ductile metals, plastic yielding often begins at impact pressures below the flow stress. Subsequent impacts deform these zones further, leading to pitting and material removal along fracture edges (Sun et al., 2023). Detailed SEM images illustrate these erosion features and mechanisms. Examination of the fracture surfaces revealed key differences in failure modes. SS304 displayed a ductile erosion mechanism, evidenced by fibrous and matte surfaces (Figure 12a), consistent with previous cavitation studies (Azhari et al., 2012). In contrast, CS1045 showed a mixed-mode erosion, with clear brittle regions characterized by flat surfaces and cleavage patterns (Figure 12b). This behavior is linked to pearlitic flaws, which act as crack initiators due to the inability of stiff cementite lamellae to accommodate plastic slip from surrounding ferrite. These flaws nucleate voids, which coalesce under plastic deformation to form cleavage fractures (Valiente et al., 2005). Because pearlite is randomly distributed, cleavage initiation is also stochastic. The BCC structure of ferritic steels makes them especially sensitive to strain rate, contributing to rapid, brittle fracture under high-velocity jet impacts (Shibata et al., 2022). Therefore, CS1045 primarily erodes through brittle mechanisms, unlike the predominantly ductile behavior of SS304. This aligns with prior observations showing that erosion in fully ferritic steels is almost entirely brittle, while duplex steels exhibit a more ductile response (Heathcock et al., 1982).

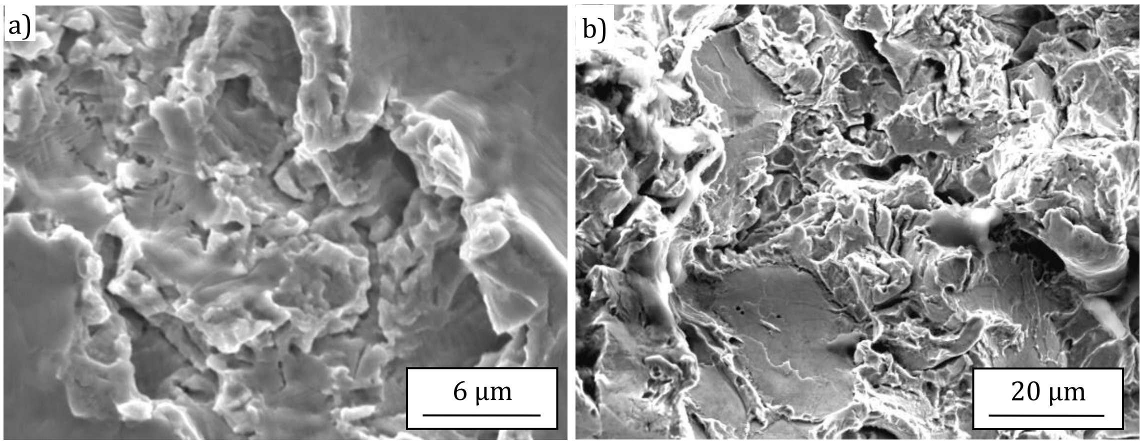

Figure 12: Representative fracture surfaces illustrating: a) a ductile erosion mechanism in SS304, and b) a mixed ductile–brittle erosion mechanism in CS1045.

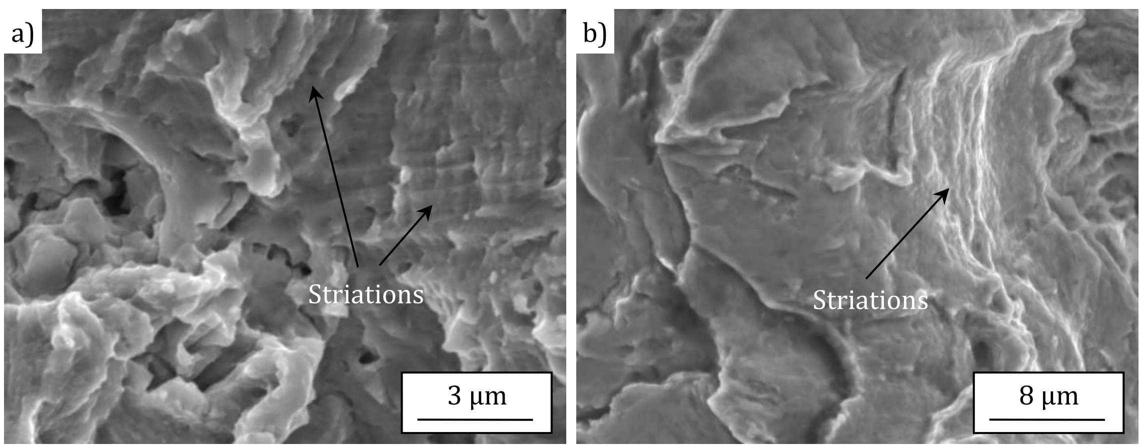

Figure 13: Striation patterns demonstrating cyclic ductile crack propagation in: a) SS304, and b) CS1045.

It is noteworthy that erosion caused by waterjet impact resembles a fatigue-driven process, particularly when the number of jet passes is increased. Rather than being the result of a single impact, erosion accumulates progressively through repeated jet strikes, resembling the cumulative nature of fatigue failure (Preece & Macmillan, 1977). Supporting this perspective, (Richman and Mcnaughton (1990) observed a strong correlation between material loss during cavitation erosion and cyclic deformation properties, reinforcing the idea that such damage is fundamentally fatigue-related. During cavitation, the continuous and random collapse of bubbles generates localized impact stresses on the material surface, comparable to those seen in low-cycle fatigue loading (Zhao et al., 1993). At a lower impact energy, the stress is insufficient to instigate immediate fracture, but localized deformation occurs at areas of stress concentration. This plastic strain accumulates over time, eventually leading to crack initiation and material failure after numerous impacts. Additionally, the radial flow of the jet contributes to the development of striation marks, particularly around the edges of impact craters, as illustrated in Figure 13.

Kamkar et al., (2013) interpreted these striations as evidence of transgranular crack propagation, indicating a cyclic fatigue-like erosion mechanism driven by the repetitive impingement of water droplets.

4.0 CONCLUSION

This study presented a comparative analysis of the surface erosion behaviour of ausenitic stainless steel 304 (SS304) and carbon steel 1045 (CS1045) subjected to waterjet surface impingement under identical processing conditions. The statistical analysis confirmed that the number of passes dominated the variation in surface roughness, while pressure, feedrate, and standoff distance contributed to secondary but meaningful effects. Hardness profiling demonstrated that CS1045 experienced significantly higher work hardening than SS304, reflecting the influence of initial material softness and microstructural composition on the response to waterjet impact. However, SS304 consistently exhibited better erosion resistance and lower surface roughness than CS1045 across a range of waterjet parameters, including pressure, number of jet passes, feedrate, and stand-off distance. The superior performance of SS304 is attributed to its higher initial hardness, ductile nature, and the ability to undergo strain-induced martensitic transformation during impingement. This phase transformation absorbs a significant portion of the impact energy, enhancing surface hardness and delaying the onset of erosion. In contrast, CS1045 showed a higher degree of surface roughening and material loss, particularly at higher pressures and with an increased number of passes. The mixed brittle–ductile erosion mode observed in CS1045 is linked to its ferrite–pearlite microstructure, which facilitates crack initiation at phase boundaries. Cleavage features, flat fracture surfaces, and micro-cracking were evident, indicating a lower capacity to accommodate repeated impact stresses. These findings highlight that erosion resistance in waterjet-treated metals is governed not only by surface hardness but also by microstructural characteristics, deformation behaviour, and the material's ability to absorb and dissipate energy. Overall, SS304 proves to be a more suitable material for applications exposed to high-pressure waterjet or cavitation environments, such as in fluid handling systems, turbine components, or marine structures. The study offers valuable insights into material selection and process optimization for erosion-critical engineering applications.

ACKNOWLEDGEMENTS

The authors gratefully acknowledge the financial support of the Ministry of Higher Education Malaysia through PGRS/1/2024/TK10/UMP/02/1 (RDU240802).

REFERENCES

Aida Husna Mohd Mahayuddin, N., Wahab, J. A., Arif Anuar Mohd Salleh, M., Faqihah Roduan, S., & Kheng Chen, H. (2020). Surface texturing method and roughness effect on the substrate performance: A short review. Jurnal Tribologi, 27.

Avilés, R., Albizuri, J., Lamikiz, A., Ukar, E., & Avilés, A. (2011). Influence of laser polishing on the high cycle fatigue strength of medium carbon AISI 1045 steel. International Journal of Fatigue, 33(11), 1477–1489.

Azhari, A., Schindler, C., Godard, C., Gibmeier, J., & Kerscher, E. (2016). Effect of multiple passes treatment in waterjet peening on fatigue performance. Applied Surface Science, 388, 468–474.

Azhari, A., Schindler, C., Kerscher, E., & Grad, P. (2012). Improving surface hardness of austenitic stainless steel using waterjet peening process. The International Journal of Advanced Manufacturing Technology, 63(9–12), 1035–1046.

Azhari, A., Schindler, C., Nkoumbou, J., & Kerscher, E. (2014). Surface erosion of carbon steel 1045 during waterjet peening. Journal of Materials Engineering and Performance, 23(5), 1870–1880.

Bansod, A. V., Patil, A. P., Verma, J., & Shukla, S. (2018). Microstructure, mechanical and electrochemical evaluation of dissimilar low Ni SS and 304 SS using different filler materials. Materials Research, 22(1), e20170203.

Barletta, M. (2011). Improvement of the fatigue behavior of stainless steel substrates by low pressure fluidized bed peening (FBP).

Bigdeli Karimi, M., Arabi, H., Khosravani, A., & Samei, J. (2008). Effect of rolling strain on transformation induced plasticity of austenite to martensite in a high-alloy austenitic steel. Journal of Materials Processing Technology, 203(1), 349–354.

Bringas, J. E. (2004). Handbook of comparative world steel standards. ASTM International.

Cao, Y. P., Cheng, S. M., Shi, W. D., Yang, Y. F., & Wang, G. W. (2022). Experimental study on surface erosion of grade A marine steel by ultrahigh-pressure water jet. Water, 14(12).

Duraiselvam, M., Galun, R., Wesling, V., Mordike, B. L., Reiter, R., Oligmüller, J., & Buvanashekaran, G. (2007). Cavitation erosion resistance of Ti6Al4V laser alloyed with TiC-reinforced dual phase intermetallic matrix composites. Materials Science and Engineering A, 454, 63–68.

Feller, H. G., & Kharrazi, Y. (1984). Cavitation erosion of metals and alloys. Wear, 93.

Field, J. E. (1999). Liquid impact: Theory, experiment, applications. Wear, 233, 1–12.

Hacini, L., Van Lê, N., & Bocher, P. (2008). Effect of impact energy on residual stresses induced by hammer peening of 304L plates. Journal of Materials Processing Technology, 208(1–3), 542–548.

Han, B., Ju, D. Y., & Jia, W. P. (2007). Influence of water cavitation peening with aeration on fatigue behaviour of SAE1045 steel. Applied Surface Science, 253(24), 9342–9346.

Hashish, M. (2024). Abrasive waterjet machining. Materials, 17(13), 3273.

Heathcock, C. J., Protheroe, B. E., & Ball, A. (1982). Cavitation erosion of stainless steel. Wear, 81.

Hu, C., He, C., Gan, X., Wan, X., Hu, F., Zhou, W., Wang, H., & Wu, K. (2022). Probing the impact of grain interior and grain boundaries on the mechanical behavior of a high-Mn austenitic steel. Journal of Materials Research and Technology, 21, 5098–5110.

Kamkar, N., Bridier, F., Bocher, P., & Jedrzejowski, P. (2013). Water droplet erosion mechanisms in rolled Ti–6Al–4V. Wear, 301(1–2), 442–448.

Kara, F., Özbek, N. A., & Özbek, O. (2025). Effect of cryogenic treatment on the machinability of Impax supreme steel and optimization of machining parameters. ES Materials and Manufacturing, 27, 1457.

Krella, A. (2005). Influence of cavitation intensity on X6CrNiTi18-10 stainless steel performance in the incubation period. Wear, 258(11–12), 1723–1731.

Krella, A. K. (2023). Degradation and protection of materials from cavitation erosion: A review. Materials, 16(5).

Lesyk, D. A., Martinez, S., Mordyuk, B. N., Dzhemelinskyi, V. V., Lamikiz, A., & Prokopenko, G. I. (2019). Effects of laser heat treatment combined with ultrasonic impact treatment on the surface topography and hardness of carbon steel AISI 1045. Optics & Laser Technology, 111, 424–438.

Mahagaonkar, S. B., Brahmankar, P. K., & Seemikeri, C. Y. (2008). Effect of shot peening parameters on microhardness of AISI 1045 and 316L material: An analysis using design of experiment. The International Journal of Advanced Manufacturing Technology, 38(5), 563–574.

Mann, B. S., & Arya, V. (2002). An experimental study to correlate water jet impingement erosion resistance and properties of metallic materials and coatings. Wear, 253.

Naeem, M., Díaz-Guillén, J. C., Khalid, A., Guzmán-Flores, I., Muñoz-Arroyo, R., Iqbal, J., & Sousa, R. R. M. (2022a). Improved wear resistance of AISI-1045 steel by hybrid treatment of plasma nitriding and post-oxidation. Tribology International, 175, 107869.

Naeem, M., Díaz-Guillén, J. C., Khalid, A., Guzmán-Flores, I., Muñoz-Arroyo, R., Iqbal, J., & Sousa, R. R. M. (2022b). Improved wear resistance of AISI-1045 steel by hybrid treatment of plasma nitriding and post-oxidation. Tribology International, 175, 107869.

Nikitin, I., & Besel, M. (2008). Correlation between residual stress and plastic strain amplitude during low cycle fatigue of mechanically surface treated austenitic stainless steel AISI 304 and ferritic–pearlitic steel SAE 1045. Materials Science and Engineering A, 491(1–2), 297–303.

Noor Fatihah Mohamad, W. W., Shahir Kasim, M., Alias, R., Izamshah Raja Abdullah, R., & Bahri Mohamed, S. (2024). Investigation of surface roughness Inconel 718 in waterjet turning. Jurnal Tribologi, 41.

Oka, Y. I., Mihara, S., & Miyata, H. (2007). Effective parameters for erosion caused by water droplet impingement and applications to surface treatment technology. Wear, 263(1–6), 386–394.

Öztürk, B., & Kara, F. (2025). Multi-objective optimization of machinability and energy consumption of cast iron depending on cooling rate. Machines, 13(2), 84.

Palová, K., Kelemenová, T., & Kelemen, M. (2023). Measuring procedures for evaluating the surface roughness of machined parts. Applied Sciences, 13(16), 9385.

Preece, C. M., & Draper, C. W. (1981). The effect of laser quenching the surfaces of steels on their cavitation erosion resistance. Wear, 67.

Preece, C. M., & Macmillan, N. H. (1977). Erosion. Annual Review of Materials Science, 7(1), 95–121.

Qutaba, S., Asmelash, M., Saptaji, K., & Azhari, A. (2022). A review on peening processes and its effect on surfaces. The International Journal of Advanced Manufacturing Technology, 120(7), 4233–4270.

Rasse, C., Mary, N., Abe, H., Watanabe, Y., & Normand, B. (2021). Role of the jet angle, particle size, and particle concentration in the degradation behavior of carbon steel under slow slurry erosion-corrosion conditions. Metals, 11(8), 1152.

Richman, R. H., & McNaughton, W. P. (1990). Correlation of cavitation erosion behavior with mechanical properties of metals. Wear.

Rossi, S., Leso, S. M., & Calovi, M. (2024). Study of the corrosion behavior of stainless steel in food industry. Materials, 17(7), 1617.

Rudawska, A. (2014). Selected aspects of the effect of mechanical treatment on surface roughness and adhesive joint strength of steel sheets. International Journal of Adhesion and Adhesives, 50, 235–243.

Shen, J., He, H., Li, Y., Zou, L., Wang, Y., Zhu, Z., Guo, L., & Fu, S. (2023). An investigation of data analysis method for hydraulic fracturing based on the water hammer effect. Unconventional Resources, 3, 284–290.

Shibata, A., Gutierrez-Urrutia, I., Nakamura, A., Miyamoto, G., Madi, Y., Besson, J., Hara, T., & Tsuzaki, K. (2022). Multi-scale three-dimensional analysis on local arrestability of intergranular crack in high-strength martensitic steel. Acta Materialia, 234.

Sun, Z. B., Liao, H. L., Wang, L. H., Jiang, L., Zhang, X., Wang, B. J., Chu, G. W., & Luo, Y. (2023). Liquid flow and breakage behaviors of two liquid jets impacting on the wire mesh with different impinging angles. Chemical Engineering Journal, 454.

Valiente, A., Ruiz, J., & Elices, M. (2005). A probabilistic model for the pearlite-induced cleavage of a plain carbon structural steel. Engineering Fracture Mechanics, 72(5), 709–728.
Wang, K., Li, C., Wang, Z., Lu, J., Li, Y., & Wang, Y. (2024). Insights into the relationship between particulate flow characteristics and local erosion behaviour under waterjet: The role of particle-fluid-surface interaction. Engineering Applications of Computational Fluid Mechanics, 18(1), 2409201.
Wang, Z., Gao, P., Han, X., & Chen, P. (2024). Surface characteristics evolution under the controllable impact cycles of an interrupted discrete waterjet. Surface and Coatings Technology, 489.
Yun, Z., Zhenkuan, S., Qilong, W., Tingchao, L., Dalei, L., & Yang, L. (2020). Improving the mechanical properties of 304 stainless steel using waterjet peening. Materials Science, 26(2), 161–167.
Zhan, K., Jiang, C. H., & Ji, V. (2012). Effect of prestress state on surface layer characteristic of S30432 austenitic stainless steel in shot peening process. Materials & Design, 42, 89–93.
Zhao, K., Gu, C., Shen, F., & Lou, B. (1993). Study on mechanism of combined action of abrasion and cavitation erosion on some engineering steels. Wear, 162, 811–819.
Zhuang, D. D., Zhang, S. H., Liu, H. X., & Chen, J. (2022). Cavitation erosion behaviors and damage mechanism of Ti-Ni alloy impacted by water jet with different standoff distances. Engineering Failure Analysis, 139.